J. Membrane Biol. 161, 131–140 (1998)

The Journal of
Membrane
Biology

Mitochondria-rich Cells and Voltage-activated Chloride Current in Toad Skin Epithelium: Analysis with the Scanning Vibrating Electrode Technique

W. Nagel, P. Somieski, A.M. Shipley*
Department of Physiology, University of Munich, Pettenkoferstr. 12, D-80336 Munich, Germany

Received: 29 May 1997/Revised: 29 September 1997

Abstract. The pathway for the voltage-activated chloride current across isolated toad skin was analyzed using a scanning 2D-vibrating voltage probe technique, which permits discrimination of local current peaks if their origins are more than 50 μm apart. The epithelium was separated from the corial connective tissue after enzymatic digestion with collagenase. Cl^- current was activated by voltage clamping the transepithelial potential to 60–100 mV, serosa positive. Activated inward current was between 85 and 450 $\mu A/cm^2$. In more than 25 tissue areas of 150 × 100 μm from 10 animals, which were automatically scanned with the vibrating probe, between 0 and 4 peaks of elevated local current (up to 800 $\mu A/cm^2$) could be identified in individual fields. The density of current peaks, which were generally located at sites of mitochondria-rich (MR) cells, was less than 10% of the density of microscopically identified MR cells. The total current across individual sites of elevated conductance was 3.9 ± 0.6 nA. Considering the density of peaks, they account for 17 ± 2.5% of the applied transepithelial clamping current. The time course of current activation over previously identified conductive sites was in most cases unrelated to that of the total transepithelial current. Moreover, initially active sites could spontaneously inactivate. The results indicate that detection of elevated current above some MR cells is not sufficient to verify these cells as the pathway for transepithelial voltage-activated Cl^- current. Since the major fraction of activated current is apparently not associated with a route through MR cells, channel-like structures in the tight junctions of the paracellular pathway must be considered as an alternative possibility. Current peaks over MR cells could be due to high density of such sites in tight junctions between MR and surrounding principal cells. Improvement of the spatial resolution of the vibrating probe is required to verify this view.

Key words: Mitochondria-rich cells — Voltage-activated chloride current — Toad skin epithelium — Scanning vibrating electrode

Introduction

Passive transepithelial movement of Cl^- across amphibian skin occurs through a highly specific, voltage-sensitive pathway, which is evidently not localized in the majority of epithelial cells, i.e., the Na^+-transporting principal cells (for review *see* [9]). As an alternative pathway, the minor moiety of interspersed mitochondria-rich (MR) cells was proposed to constitute the morphological site for this transport [8, 12]. Originally based on indirect evidence of the correlation between MR-cell density and Cl^--conductance [22] or speculation on hormonal effects on the different pathways [7], the idea was strongly supported by the observations of extracellular current peaks above MR-cells [5, 6] and the demonstration that intracellular volume of MR-cells was responsive to an alteration of transcellular Cl^- movement [13, 21]. According to these data and subsequent computer modeling, voltage-sensitive Cl^- channels in the apical membrane of MR-cells could provide the route for Cl^- through a cellular compartment. Although conceptually fascinating, the localization remains questionable in view of results from electron probe microanalysis. Using this technique, which is also able to localize the routes of transported ions in complex tissues, it was demonstrated that MR-cells represent a very inhomogeneous compartment with regards to intracellular electrolyte concentrations. Furthermore, uptake of Br^- as a marker for Cl^- transport was observed in a certain fraction of MR-cells only, whereas the majority of MR-cells was unrelated to

* *Present address:* 22 Buckingham Drive, Sandwich, MA 02673, USA

Correspondence to: W. Nagel

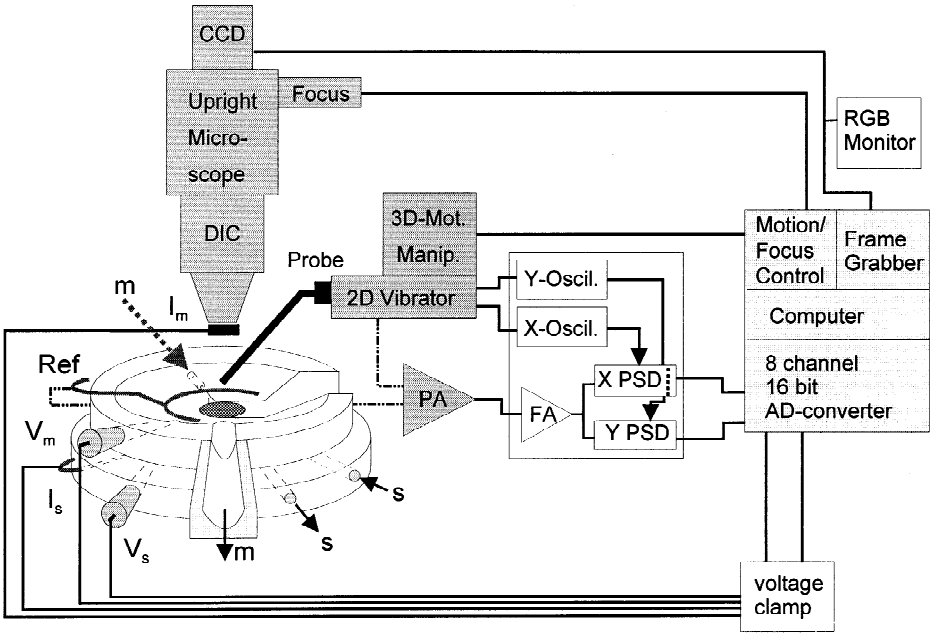

Fig. 1. Schematic drawing of the experimental setup. The modified Ussing chamber is shown with the electrodes for voltage determination (V_m,V_s) and current sending (I_m,I_s), which are connected to the automatic voltage clamp unit. Fluid inlets are represented by arrows labeled *m* and *s*. The mucosal half chamber has an overflow directed by a cotton string. Perfusion of the serosal half chamber was gravity driven; the hydrostatic pressure at the serosal outlet could be adjusted to slightly negative values to fix the tissue to the supporting grid without notable indentation. Local voltage gradients were recorded with the 2D-vibrating probe, mounted on a 3D micro-stepping motor manipulator. The probe is vibrated with 2 orthogonal piezo bimorphs. The main elements of the vibrating probe system are preamplifier (PA), filteramplifier (FA), phase-sensitive detectors (X-PSD, Y-PSD) and sine/cosine oscillators (X-Oscil., Y-Oscil.), connected via a 16-bit AD converter to the computer. The chamber was mounted under an upright DIC microscope equipped with a CCD camera connected to a RGB monitor and the computer via a frame grabber.

transepithelial Cl^- movement [3, 15, 17]. These observations and other indirect evidence raise the question whether the specific transport sites for passive Cl^- movement might be located in the tight junctions of the paracellular pathway [14].

For appropriate evaluation of the supposed pathway through MR-cells, it should be recalled that previous publications on current peaks above MR-cells [5, 6] are based on a rather small number of observations, which show considerable variation among different skins and within individual preparations. A systematic analysis of the distribution of conductive *vs.* electrically inactive MR-cells was not done. Furthermore, local current density could not be compared to the overall transepithelial Cl^- current, since the experimental setups were apparently not equipped with the necessary voltage/current recording systems. These limitations led us to reinvestigate the question of local distribution of voltage-activated Cl^- current across toad skin using improved vibrating probe techniques along with careful determination of the transepithelial electrical parameters. Our results show that elevated current density may indeed be observed in the extracellular spaces above MR-cells but the number of conductive sites and the magnitude of the local current are much less than necessary to account for the simultaneously recorded transepithelial Cl^- current. Routes other than MR-cells must thus be considered for transepithelial Cl^- movement.

Materials and Methods

The experiments were done on isolated abdominal skins from *Bufo viridis* collected in Israel. Prior to the experiments, the animals were kept between 2 and 12 weeks in the laboratory at room temperature with free access to distilled water. They were fed every week with meal worms *ad libitum.* The animals were sacrificed by double pithing, and the skin was carefully dissected. After gently scraping the corial side of the skins with a scalpel, small lucite gaskets (15 mm diameter) were glued to the mucosal surface with cyanoacrylate adhesive (Histoacryl, Braun, Melsungen, Germany) and the serosal side was exposed to a Ringer solution with 1 mg/ml collagenase (Type I, Sigma, St. Louis, MO) for 60–75 min. Thereafter, the connective tissue could be easily removed with fine forceps under microscopic control. Tissues stored in Ringer's at 4°C retained voltage-sensitive Cl^- conductance for more than 24 h.

Isolated epithelia were mounted mucosal side up in a modified Ussing chamber, which is schematically depicted along with the main electronic parts of the system in Fig. 1. The tissue was supported on the serosal side by a resi-insulated gold-plated REM grid (mesh width 300 × 300 μm, Plano, Marburg, Germany). The exposed tissue area was 0.28 cm^2. Edge damage was minimized by covering the edge of the mucosal half chamber with heavy silicone grease. Matched Ag/AgCl electrodes were connected to both halves of the chamber via 0.5 M KCl bridges terminating 0.5 mm apart from the serosal or mu-

cosal surface, respectively. To pass current, a circular Ag wire electrode was built into the serosal half chamber 2.5 mm apart from the tissue. As a current return, another circular Ag wire was formed around the water immersion lens. This electrode, which contacted the apical perfusion solution, was 2.0 mm apart from the apical surface, when the tissue was in focus. Both electrodes were carefully chlorided before each experiment to ensure homogeneous field distribution. The tissue was continually perfused on both sides with fresh Ringer solution of the following composition (in mM: Na^+ 112, K^+ 2.5 Ca^{2+} 1, Cl^- 114, HEPES 3.7; pH = 7.5). All solutions were filtered through 0.2 μm membrane filters (Sartolab V500, Sartorius, Göttingen, Germany). To prevent air bubbles from forming in the serosal chamber, the serosal perfusion solution was equilibrated with O_2 at about 40°C and thereafter brought to the experimental temperature of 22–25°C. The mucosal perfusion solution was aerated with air. Perfusion rates of mucosal and serosal side were 5 and 2 ml/min, respectively. The mucosal perfusion solution always contained amiloride (10^{-5} M).

Electrical determinations were done with a custom-built automatic voltage clamp system [16]. Transepithelial potential difference (V_t) was referred to the mucosal side as ground and transepithelial current (I_{macro} or macro current) was considered positive for anion flow from mucosa to serosa. To determine tissue conductance (g_t), voltage pulses of 10 mV were applied for 200 msec every 2 sec and used for online analog estimation according to $g_t = \Delta I_t/\Delta V_t$. Conductance determination had to be interrupted during vibrating probe analysis to avoid transient artifacts in the vibrating probe data. In these cases, g_t was estimated from the magnitude of the clamp current in the presence of a constant holding potential.

The chamber was placed under an upright microscope equipped with a water immersion DIC lens (Zeiss Axioscope FS with 40×/0.75 W and achrom.-aplan. condensor 0.9 NA). A low light CCD video camera (Burle TC355) connected to a frame grabber (ComputerEyes 1024), provided video image storage and real time video display of the specimen on a video monitor (Sony PVM-1341). A 3D linear motor driven manipulator (MM33, Märzhauser, Wetzlar, Germany) allowed for positioning of selected tissue areas. The vibrating voltage electrode was mounted on a 3D micro-stepping motor manipulator system (CMC-4, Applicable Electronics, Sandwich, MA) and could be controlled by the data acquisition program (*see below*). The whole setup was mounted on a vibration isolated air table, which avoided any contact with parts that had to be manipulated during the experiments, and was enclosed in a faraday cage.

A 2-dimensional vibrating voltage probe system (SVM-200, Applicable Electronics, Sandwich, MA) based on that described by Scheffey et al., 1991 [19] was used to measure the extracellular current distribution above the epithelium. Transepithelial current produces voltage gradients in the extracellular fluid above the tissue, which are proportional in magnitude to the local current. Vibrating a voltage probe in these electrical fields yields ac-signals, at the same frequency as the vibration, with amplitudes proportional to the local current. The potentials were recorded with stainless steel electrodes (SS300301, Micro Probe, Clarksburg, Md). They were electroplated with gold and platinum black as described [18] to a tip diameter of 10–15 μm which provides a capacitive coupling to the medium. Electrodes were mounted to a piezoelectric vibrator assembly and vibrated in two precisely adjusted orthogonal directions with frequencies of 200–400 Hz parallel to the tissue surface (x-direction) and 300–600 Hz perpendicular to the surface (y-direction). With vibration amplitudes of 10–15 μm, probe signals were in the range of μV. These probe signals were passed through two phase-sensitive detector amplifiers, adjusted to the phase of each vibration frequency. In-phase signals corresponding to the local current flow were filtered and fed to a computer via a 16-bit AD-board (CIO-DAS-1602/16, ComputerBoards, Mansfield, MA). Additional phase-sensitive amplifiers, adjusted to be 90° out of phase (quadrature) in each vibration direction were used to verify that the phase of the probe signal was constant and actually reflected the local electric field. During operation, the quadrature signal must be zero, whereas any increase would indicate touching the tissue with the probe or some other artifact.

Vibrating electrodes were calibrated with known constant current delivered from a 3M KCl-filled glass electrode with a 2 μm tip diameter. The calibration procedure was usually carried out in the Ussing chamber without voltage clamping the tissue and with the vibrating probe at least 500 μm above the tissue. The baseline signal of the probe was repeatedly adjusted during the experiments; transepithelial current clamping was interrupted for this determination. As additional test for the accuracy of current determinations with the vibrating probe, the total current flow in all scanned areas was estimated by summation of the local current. Unless this value was within ±20% of the simultaneously measured transepithelial current, the determination was disregarded.

All vibrating probe signals were processed using software, which calculated local current, angle and current vector (ASET version 1.0, Science Wares, Falmouth, MA). probe positioning, automatic scanning of selected tissue areas, storage of data and video images, and vector overlays were also controlled by this software. Data are presented using commercial graphic software (Origin, Microcal, Northamptom, MA).

Mean values are reported ± SEM. Significance of difference is calculated using Student *t*-test, considering $P < 0.05$ as significant.

Results

The voltage-activated conductive Cl^- pathway was analyzed by perturbation of the transepithelial PD between slightly negative (−30 mV) and moderately positive (+60 to +100 mV) values, which leads to virtually complete inactivation and almost maximal activation, respectively [11]. For a meaningful analysis, it was essential that the transepithelial clamping current (macro current) was reliably recorded by the vibrating probe (probe current) in areas of homogeneous distribution, i.e., at sufficient distance from the epithelial surface. Figure 2*A* shows that this requirement was fulfilled. When the tip of the vibrating probe was located 250 μm above the tissue surface, the time course and magnitude of the induced voltage-activated Cl^- current was correctly measured by the probe. Furthermore, the probe current was unchanged when the probe was moved horizontally ±100 μm (1,2), indicating homogeneous distribution at this distance above the tissue surface. Similar observations were made in 24 trials during 15 experiments. On the average, the ratio of probe current at a homogeneous level to the macro current was 1.08 ± 0.19 and not significantly different from unity. Figure 2*B* shows observations with the probe positioned 30 μm above the tissue surface at a location with low probe current, which was in this case a tissue area lacking MR-cells. Local current was lower than the macro current during activation, but the time courses of I_{probe} and I_{macro} did not differ notably. When the probe was 30 μm above the location of a swollen MR-cell in an area with a high density of MR-cells (Fig.

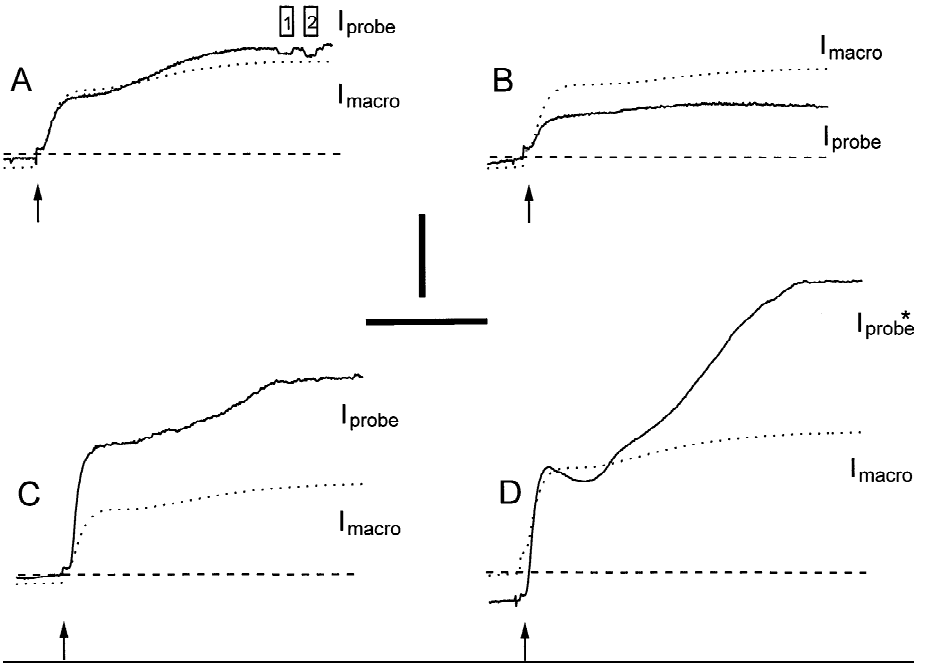

Fig. 2. Time course of transepithelial macro-current (I_{macro}) and local vibrating probe current (I_{probe}) during voltage activation of Cl^- current in toad skin. Recordings labeled *A-D* represent determination at 250 μm above the tissue surface (*A*), 35 μm above the surface at a low current site (*B*), 35 μm above the surface of a swollen MRC (*C*), 35 μm above the surface at a previously identified ''hot spot'' (*D*). Boxes (1 and 2) on top of *A* designate horizontal movement of the probe by ±100 μm. The vertical and horizontal bar indicate current density of 100 $\mu A/cm^2$ and 5 min, respectively. In *D*, scale for I_{probe} is reduced to 40%. Before each recording, I_{probe} was adjusted to zero during a brief open-circuit period; V_t of the amiloride-treated tissue was then below 2 mV. Voltage clamping the tissue to −30 mV required a clamp current of $-6\ \mu A/cm^2$. Arrows indicate perturbation of V_t from −30 mV to +80 mV. The Na^+ current was blocked by 10^{-5} M amiloride.

2*C*), the time course of current activation was nearly identical for I_{macro} and I_{probe}, the latter being almost twice as large as I_{macro} throughout. Different patterns were obtained with the probe at a height of 30 μm above a previously identified ''hot spot'' (Fig. 2*D*), where the probe current was much larger than the macro current during the development and after full activation of I_{Cl}. Furthermore, the time course of change in probe current during activation was notably different from that of the macro current, displaying a rapid initial gain and a subsequent slow increase to a final steady state.

Similar observations during activation/inactivation cycles were made in all tissues, when the vibrating probe was located above the center of a previously identified ''hot spot.'' Figure 3 shows typical observations. It is evident that a synchronous increase in I_{macro} and I_{probe} was seldom observed. As would be expected for unrelated transport sites, response patterns varied in either direction. Occasionally, we found that initially responsive sites were silent in later activation tests and that some active sites turned off during the measurement. In some cases, an instantaneous change of I_{probe} to a final steady-state level was observed; these sites also displayed simple ohmic current responses to perturbation of voltage. Instantaneous changes in I_{probe} and ohmic current/voltage relationships were observed in a few cases above gland pits. The majority of glands were electrically inactive, irrespective of the presence or absence of an intact glandular body.

To localize the source of ''hot spots,'' recording of the local current vectors has the advantage that, in addition to the magnitude of current flow, changes in the angle of current flow indicate the position of the probe relative to the source of the current. This is shown in Fig. 4 for a ''hot spot'' in a voltage-activated tissue. The probe was previously adjusted to pass over the center of the ''hot spot'' and then advanced as close as possible to the tissue surface (probe center at 12 μm). During the linear scan, current vectors changed from 70° to 140°C, transition of the center (90°C) occurred with movements of less than 3 μm. The center of current cannot be discriminated from the location of a MR-cell. Note, however, that this was not the large MR-cell visible slightly below the series of current vectors, which turned out to be electrically inactive. Similar patterns of current vectors were obtained in more than 50 cases. Occasionally, and particularly with a small distance between the probe and the tissue, the profile displayed a plateau with a width of 10–15 μm, which had an essentially constant vector angel of 90°C. Morphological sites related to these plateaus could not be resolved.

The spatial resolution of the present technique was

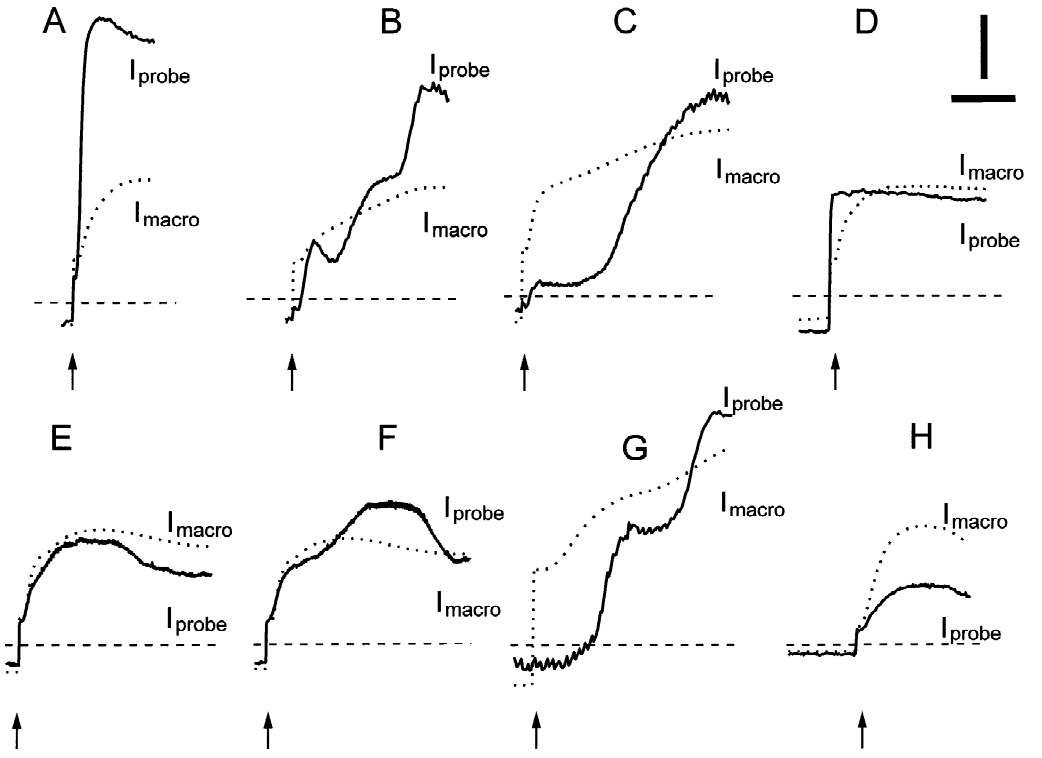

Fig. 3. Time course of voltage-induced activation of local current (I_{probe}) at previously identified ''hot spots'' in relation to the response of transepithelial clamping current (I_{macro}). Arrows indicate the perturbation of V_t from −30 to +80 mV. The Na^+ current was blocked by 10^{-5} M amiloride.

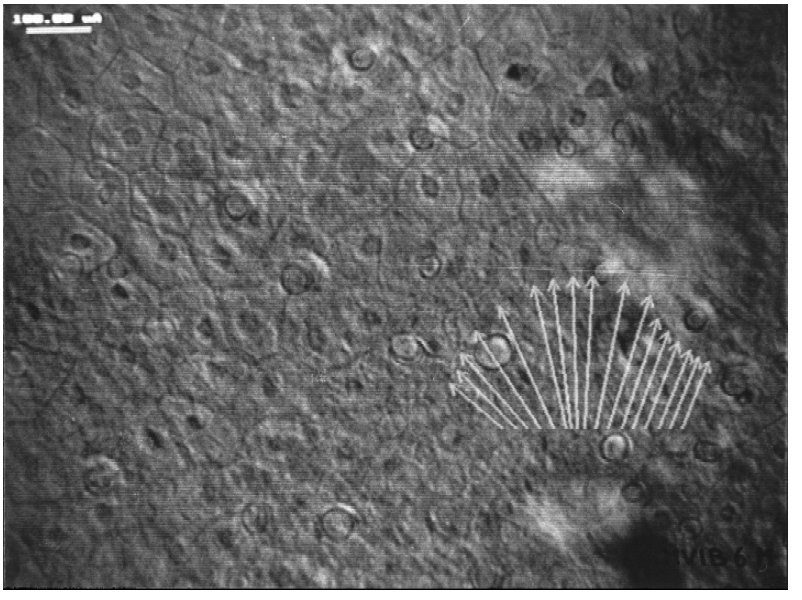

Fig. 4. Representative vector line-scan of a voltage-activated ''hot spot'' overlaid on the DIC image of a split toad skin. The depicted video image reflects a tissue area of 320 × 240 μm. During determination of the current vectors, the probe was located at the base of the respective arrows. The horizontal bar in the upper left corner indicates current density of 100 μA/cm^2. Overall transepithelial current at the clamp potential of 80 mV was 135 μA/cm^2.

estimated from linear scans over ''hot spots.'' Figure 5 shows typical observations along with contour plots of the probe current obtained at two different distances (30 and 17.5 μm) between the probe tip and tissue surface. The white lines represent line scans across the hot spots shown above the contour plots. With the closer probe position, two distinct bell-shaped current peaks with a distance of 40 μm between their centers could be discriminated. At the farther distance, the associated ''hot spots'' were superimposed, which produced an elongated

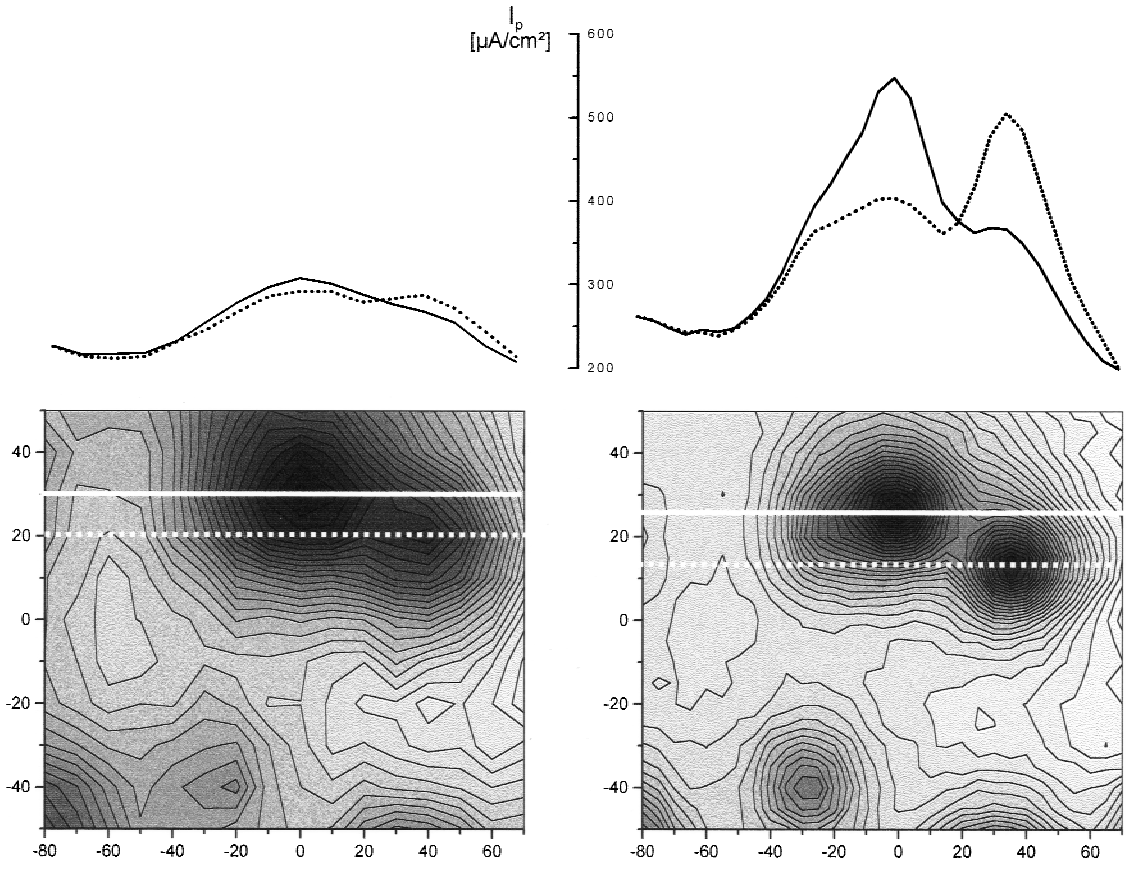

Fig. 5. contour plot of current distribution in a field of 150 × 100 μm. The distance between the tip of the vibrating probe and the tissue surface was 30 μm (left section) and 17.5 μm (right section). Cl^- current was activated by voltage perturbation to 80 mV, serosa positive. The white lines in the surface plots indicate the pathway of the probe corresponding to the respective current profile in the upper panels. I_{macro} was 225 μA/cm^2.

plateau with the same width and twice the length as the discriminate peaks. The half-width of individual peaks as estimated from 23 line scans at distances of 17.5 to 40 μm between probe tip and tissue was 46 ± 12 μm. In every case, the shapes of the local peaks were rotationally homogeneous. This would agree with an origin from a single current source according to the current distribution equation. The maximal magnitude of local current peaks was variable but with little dependence on the level of voltage-activated transepithelial current; in some experiments, peak values were above 800 μA/cm^2.

The frequency and distribution of local current peaks was analyzed in numerous microscopic fields. Figure 6 shows from a representative experiment surface and contour plots of the local current along with the video image of the investigated tissue area. Clamp current in the activated state (+80 mV) was 90 μA/cm^2. The vibrating probe, scanning in steps of 10 μm at a vertical distance of 20 μm above the tissue surface, detected one single location of elevated current in the field of 150 × 100 μm; peak current was 297 μA/cm^2. Probe current at peak-free areas was notably less than the macro current (56 ± 13 μA/cm^2). The video image showed approximately 30 MR-cells in the scanned area (not all MR-cells are visible in the video image). Thus, most MR-cells are not associated with elevated local current. Similar results were obtained in all experiments. Mean values are summarized in the Table, which indicates that the density of current peaks was less than 10% of the density of MR-cells, i.e., that the majority of MR-cells did not show elevated current flow. Using the density of current peaks in scanned areas and the current flow across individual sites (I_s), the total magnitude of current flow through ''hot spots'' (I_s^{total}) was estimated. The values of I_s were obtained by integration of the current profile at the ''hot spot.'' Line scans in two orthogonal directions had demonstrated that the peaks could be assumed rotationally symmetric and that they could be fitted to Gauss curves. This enabled to determine the volume of a 3-dimensional Gauss curve (bell) as a measure of the current through the respective peak. The individual values shown in the Table are the means of 4–9 determinations from different fields of a single tissue. On the average, a current of 3.9 ± 0.6 nA was

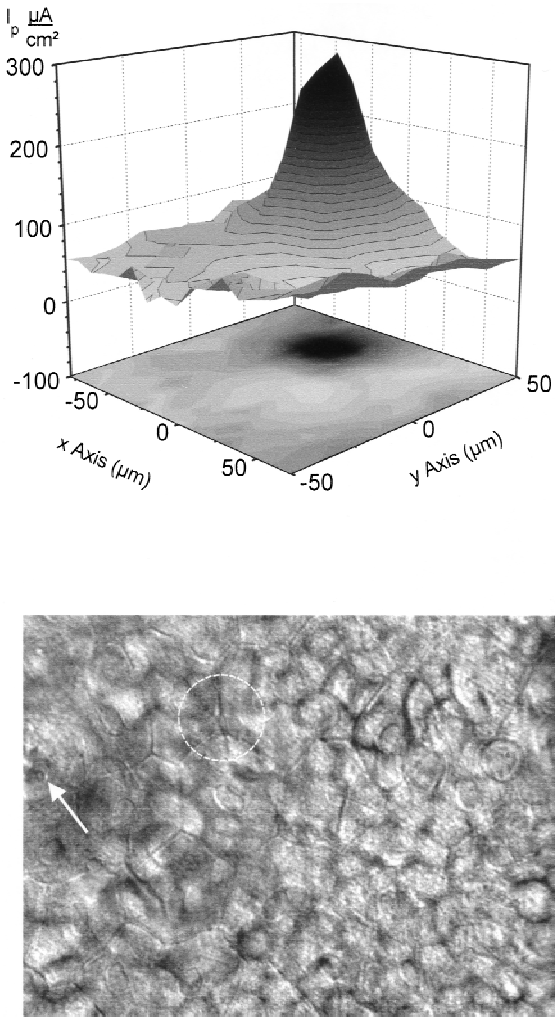

Fig. 6. Surface plot after activation of Cl^- current by voltage perturbation to 80 mV of a field of 150 × 100 μm shown in the video image. I_{macro} was 90 μA/cm^2. The location of the single active site is labeled by the hatched circle in the video image. NOTE: The gland marked by the arrow on the left side in the video image was not conductive.

observed at activated site. The total current across active sites was very variable, both in its magnitude and in relation to the simultaneously measured value of transepithelial clamping current (I_{macro}). Except for one experiment, however in which only one single area with particularly many active sites (5) was scanned and 29% of I_t would be accounted from these estimation, the current across ''hot spots'' was less than 25% of the transepithelial current, averaging 17.0%. It has to be added that numerous area scans done in the listed tissues did not show current peaks. In other cases, peaks were situated at the border of the field and could not be evaluated. This implies that the actual ratio between current through active sites and transepithelial Cl^- current is presumably less than the given value.

Discussion

Meaningful conclusions regarding the localization of pathways for Cl^- movement across amphibian skin can only be derived from techniques that permit correlation of morphological data with transport parameters. Hitherto, four methods have been applied: electron probe microanalysis [3, 15, 17], intravital micromorphometry [13, 21], analysis of extracellular current density [5, 6] and patch-clamp techniques [10, 20]. All of these techniques have demonstrated finite Cl^- permeability of apical and basolateral membranes of MR-cells. In contrast to principal cells, which do not show measurable apical Cl^- conductance [16, 23], MR-cells may thus be a pathway for passive, transepithelial Cl^- transport. The quantitative significance of this route, however, remains unsolved. Our data using the vibrating voltage probe in conjunction with transepithelial current determination, demonstrate that current peaks in the extracellular space above the toad skin account for less than 15% of the voltage-activated transepithelial Cl^- current. Due to limited spatial resolution of the probe we could not resolve whether these ''hot spots'' were really associated with MR-cells. More momentous is the finding that the major faction of Cl^- current was not related to MR-cells. Since previous pharmacological and kinetic analyses contradict the possibility of more than a single kind of Cl^- movement across amphibian skin, we have to imply that MR-cells are not the pathway for transepithelial electrodiffusive Cl^- transport. This conclusion is not unexpected from previous electron probe microanalyses, which show notable uptake of Br^- from the apical side (as a measure of Cl^- movement) under conditions of voltage activation in 15 to 25% of the MR-cells in the epithelium. Assuming that uptake into MR-cells reflects transcellular movement, the rate was considered insufficient to accomplish the transepithelial anion current [3, 15]. Rick [17] found a larger fraction of MR-cells with voltage-induced Br^- uptake in a selected group of frog skins, but the variation was similarly evident.

Previous determinations of local current above MR-cells are difficult to evaluate for several reasons. (i) The number of observations is small or uncertain. Foskett & Ussing [5] observed 15 peaks from 30 examined cells in 2 or 3 tissues. An unspecified number of tissues did not show peaks. Katz and Scheffey [6] made a crude estimate that 30–90% of MR-cells in their preparation did show current peaks, but no numbers are given. (ii) Correlation between local and overall current is impossible since transepithelial current is not reported. This is particularly problematic as the animals were pre-adapted in NaCl to reduce the density of MR-cells. (iii) It is questionable whether the magnitude of current over ''hot spots'' in both studies can account for the total transepithelial current. Foskett and Ussing [5] give a ''rough estimate'' of 1 pA/μm^2 (equivalent to 100 μA/cm^2) at

Table. Summary data of area scans with the vibrating voltage probe

MR-cells [$\times 10^3/cm^2$]	Active sites [$\times 10^3/cm^2$]	I_s [nA]	I_s^{total} [$\mu A/cm^2$]	I_{macro} [$\mu A/cm^2$]	I_s^{total}/I_{macro} $\times 100$ [%]
71	1.7	5.4	9.1	173	5.3
255.6	13.3	3.2	42.6	313	13.6
43.7	4.2	5.5	23.1	132	17.5
129.2	25.7	2.5	66.8	270	24.7
95.5	13.3	1.7	22.6	208	10.9
110.4	5.2	5.9	30.8	297	10.4
314.6	26.7	4.9	130.8	450	29.1
120.8	7.7	5.6	43.1	180	23.9
94.4	3.8	1.5	5.7	85	6.7
138.6	13.3	2.4	29.8	163	18.3
137.4 ± 26.5	11.5 ± 2.8	3.9 ± 0.6	40.4 ± 15	227 ± 34	17.0 ± 2.5

Density of MR-cells and active sites were estimated from video images and scan plots, respectively. Current at active sites (I_s) is calculated as the volume of 3D Gauss curve of the peak; each value represents the mean of 4–9 determinations in 1–4 different scanned areas. The total current at active sites (I_s^{total}) is the product of columns 2 and 3. Transepithelial current (I_{macro}) is the mean value of clamping current during the determinations of I_s. The volume of the 3D Gauss curve was calculated with the equation $V = (\pi/2)^{0.5} \cdot 2 \cdot \sigma \cdot A$. ($A$: area of Gauss curve; σ: standard deviation). Mean values are reported ± SEM.

100 mV clamp potential over individual MR-cells. In view of the small number of ''hot spots,'' the total current from these peaks must have been rather low. Katz and Scheffey [6] report peak values of 15–20 $\mu A/cm^2$ over active MR-cells. These peaks, if existing over 10% of the macroscopic epithelial area (which is an unrealistically high assumption), would explain less than 5 $\mu A/cm^2$ in the voltage-activated state. That is clearly not feasible. Irrespective of these uncertainties and shortcomings, however, both previous reports lead to the same conclusion as the present study, i.e., that the number of conductive sites is much smaller than the number of MR-cells.

Quantification in the present study is based on the density of conductive sites and the mean value of local current in identified peaks. The density of conductive sites was determined by automatic scanning (in steps of 5–10 μm) of selected areas (150 × 100 μm) with a microstepping motor manipulator and continuous data acquisition. On the average, the density of current peaks was $11.5 \pm 2.8 \times 10^3/cm^2$. In the same tissues, the density of MR-cells as estimated from computer-stored DIC-images averaged $137 \pm 26 \times 10^3$ cells/cm^2, which is in the same range as in previous studies [23]. If observed current peaks were originating from MR-cells, high current would flow through less than 10% of the MR-cells. The current at active sites could not be calculated by the technique of Foskett and Machen [4], which requires precise knowledge of the size of conductive spots and the distance between the current source and the vibrating probe. As an alternative method we have obtained Gauss fits of the local current observed during line scans through the center of active sites. These Gauss curves were found to be rotationally symmetric, and the total current across the site, which is equivalent to the volume of the Gauss bell, could be estimated using standard algorithm. As a test for proper detection of local current by the probe (I_{probe}) and homogeneity of current flow, I_{probe} was frequently measured when the probe was elevated to more than 200 μm above the tissue. At this position, peaks could never be detected, and I_{probe} was not significantly different from the transepithelial current.

The width of current peaks was dependent on the distance between the vibrating probe and the tissue. At the usual distance of 30 μm above the epithelial surface, the half-width of peaks was 46 ± 12 μm. This would permit the separation of current sources, which are more than 50 μm apart. At the average density of 137×10^3 MR-cells/cm^2, the distance between evenly distributed MR-cells is about 30 μm. The spatial resolution of the vibrating probe is thus insufficient to identify the current status of individual MR-cells. Actually it shows that current peaks are considerably more than 50 μm apart. Origin from clusters of narrow spaced MR-cells can be excluded, since peaks were generally found above or in the vicinity of segregate MR-cells whereas areas with high density of MR-cells were lacking elevated current. Current peaks could indicate that only a small fraction of MR-cells is activated by voltage clamping to serosa positive potentials. These cells had to allow the passage of current of about 4 nA Cl^- current per cell, which is twice as large as the value derived from a correlation between voltage-activated Cl^- current and density of MR-cells [23] and four times larger than estimated using a vibrating voltage probe [5]. Nevertheless, it cannot account for the transepithelial current flow, since active sites occur at less than 10% of the density of MR-cells. This is

contrary to the previous assumption of complete and homogeneous participation of MR-cells [9] and has the consequence, that less than 20% of the transepithelial Cl^- current can be explained. The background current close to the tissue surface was typically 70–90% of the transepithelial current, and was not notably related to the local density of MR-cells. Closer approach of the probe to the tissue surface did not reveal additional current peaks. These observations argue against passage of Cl^- current through MR-cells, but cannot rule it out. Considering the diameter of 12–15 μm of the vibrating probe and the morphology of amphibian skin, which shows a *stratum corneum* of 4–8 μm thickness above the first living cell layer, approach to less than 25 μm above the actual outer border was not possible during the area scans of the present study. At this distance from the putative sources of current, the local differences of the electrical field can be such much levelled that the original distribution is no more visible. Use of vibrating electrodes of smaller size along with means to reduce the thickness of the *stratum corneum* and careful alignment of the tissue will be necessary to resolve this problem.

The temporal response of local current at active sites was usually different from the time course of the clamp current. Among these observations was occasionally that I_{probe} changed with a sudden jump to the final level, whereas I_{macro} showed the usual slow time course. Furthermore, *I/V* relationships of the local current were strictly linear at all levels of voltage. Such response patterns suggest that the probe was located above a dead cell in the outermost reactive layer of the tissue. Such cells, which resemble MR-cells in shape and position, have occasionally been observed with the electron microprobe (A. Dörge, *personal communication*). In most cases, glands were electrically tight, regardless of whether the whole gland was preserved or merely a short length of the glandular duct was present. On rare occasions, high peaks were observed over glands. Instantaneous response to voltage perturbation and a linear *I/V* relationship, in addition to the morphological situation, easily distinguished these locations from voltage-sensitive ''hot spots.'' Conductive gland sites as well as the above ''dead cells'' were not considered in the present analysis.

We have noted that the size of MR-cells was affected by voltage perturbation. Whereas MR-cells were often hardly detectable in the inactivated state, they became evident briefly after voltage clamping to 80 mV and seemed to increase in size before the activation of transepithelial Cl^- current was complete. The data shown by Foskett and Ussing [5] reveal similar response patterns. Estimates of MR-cell volume could not be made with the optical system used, but it turned out that these morphological changes were unrelated to the existence of local current peaks. It is beyond the scope of the present study to elucidate the relation between volume reactions of MR-cells and transcellular Cl^- current, which has promoted the idea of a Cl^- conductive pathway across these cells [13].

In doubt of the passage of the voltage-activated Cl^- current through MR-cells, it is necessary to consider the only remaining route across the epithelial layer, i.e., the tight junctions of the paracellular pathway. This pathway is usually considered to be extremely impermeable, since leak fluxes in the absence of Cl^- are very low [2]. This property, however, is unrelated to the actual problem. If the permeable substrate is absent or if the pathway cannot be activated because it is lacking some necessary factor, missing permeation does not exclude its existence under the appropriate conditions. The problem is thus primarily whether tight junctions may contain ion-selective structures comparable to membrane channels, which are activated under certain conditions to generate specific permeation pathways across the tight seals between the epithelial cells. Considering the elaborate composition of tight junctions and the numerous identified elements for their regulation (for review *see* [1]), the presence of channel-like structures, which may change between open/closed conformation, appears possible. Regulation of these permeation sites could be linked to MR-cells. This could explain the location of ''hot spots'' in the vicinity of MR-cells, and it cannot be ruled out that they originate from exceptionally high permeability of the tight junctions around certain MR-cells. Improvement of the local resolution of the vibrating probe along with attempts to access the actual surface of the outermost living cell layer may solve these problems.

We are grateful to Dr. Peter Smith for the permission of a preliminary study using the National Vibrating Probe Facility at the Marine Biological Laboratories, Woods Hole, MA. The kind help of Prof. Uri Katz, Technion, Haifa in providing *Bufo viridis* and valuable comments during preparation of the manuscript are gratefully acknowledged. The work was supported by grants from the Deutsche Forschungsgemeinschaft and generous equipment loans by Applicable Electronics, W. Yarmouth, MA, and Science Ware, Falmouth, MA.

This study is part of investigations carried out by Ms. Petra Somieski for her doctoral thesis in the Faculty of Medicine, Ludwig-Maximilians-University, Munich.

References

1. Anderson, J.M., Van Itallie, C.M. 1995. Tight junctions and the molecular basis for regulation of paracellular permeability. *Am. J. Physiol.* **269:**G467–G475
2. Bruus, K., Kristensen, P., Larsen, E.H. 1976. Pathways for chloride and sodium transport across toad skin. *Acta Physiol. Scand.* **97:**31–475
3. Dörge, A., Rick, R., Beck, F.X., Nagel, W. 1988. Uptake of Br in mitochondria-rich and principal cells of toad skin epithelium. *Pfluegers Arch.* **412:**305–313
4. Foskett, J.K., Machen, T.E. 1985. Vibrating probe analysis of teleost opercular epithelium: correlation between active transport

and leak pathways of individual chloride cells. *J. Membrane Biol.* **85:**25–35

5. Foskett, J.K., Ussing, H.H. 1986. Localization of chloride conductance to mitochondria-rich cells in frog skin epithelium. *J. Membrane. Biol.* **91:**251–258
6. Katz, U., Scheffey, C. 1986. The voltage-dependent chloride current conductance of toad skin is localized to mitochondria-rich cells. *Biochim. Biophys. Acta* **861:**480–482
7. Kristensen, P. 1981. Is chloride transfer in frog skin localized to a special cell type. *Acta Physiol. Scand.* **113:**123–124
8. Kristensen, P. 1982. Chloride transport in frog skin. *In:* Chloride Transport in Biological Membranes. J.A. Zadunasky, editor. pp. 319–332. Academic Press, New York
9. Larsen, E.H. 1991. Chloride transport by high-resistance heterocellular epithelia. *Physiol. Rev.* **71:**235–283
10. Larsen, E.H., Harvey, B.J. 1994. Chloride currents of single mitochondria-rich cells of toad skin epithelium. *J. Physiol.* **478.1:** 7–15
11. Larsen, E.H., Kristensen, P. 1978. Properties of a conductive cellular chloride pathway in the skin of the toad (*Bufo bufo*). *Acta Physiol. Scand.* **102:**1–21
12. Larsen, E.H., Rasmussen, B.E. 1982. Chloride channels in toad skin. *Phil. Trans. Roy. Soc. Lond. B.* **299:**413–434
13. Larsen, E.H., Ussing, H.H., Spring, K.R. 1987. Ion transport by mitochondria-rich cells in toad skin. *J. Membrane Biol.* **99:**25–40
14. Nagel, W. 1989. Chloride conductance of amphibian skin. Localization to paracellular pathways. *Miner. Electrol. Metabol.* **15:** **1**163–170
15. Nagel, W., Dörge, A. 1990. Analysis of anion conductance in frog skin. *Pfluegers Arch.* **416:**53–61
16. Nagel, W., Garcia-Diaz, J.F., Essig, A. 1983. Cellular and paracellular conductance patterns in voltage-clamped frog skin. *In:* Membrane Biphysics II. Physical Methods in the Study of Epithelia. M.A. Dinno, A.B. Callahan and T.C. Rozzell, editors. pp. 221–231. Alan R. Liss, New York
17. Rick, R. 1994. Short-term Bromide Uptake in Skins of *Rana pipiens. J. Membrane Biol.* **138:**171–179
18. Scheffey, C. 1988. Two approaches to construction of vibrating probes for electrical current measurement in solution. *Rev. Sci. Instrum.* **59:**787–792
19. Scheffey, C., Shipley, A.M., Durham, J.H. 1991. Localization and regulation of acid-base secretory currents from individual epithelial cells. *Am. J. Physiol.* **261:**F963–F974
20. Sörensen, J.B., Larsen, E.H. 1996. Heterogeneity of chloride channels in the apical membrane of isolated mitochondria-rich cells from toad skin. *J. Gen. Physiol.* **108:**421–433
21. Spring, K.R., Ussing, H.H. 1986. The volume of mitochondria-rich cells of frog skin epithelium. *J. Membrane Biol.* **92:**21–26
22. Voute, C.L., Meier, W. 1978. The mitocondria-rich cell of frog skin as hormone-sensitive ''shunt-path''. *J. Membrane Biol.* **40:** 151–165
23. Willumsen, N.J., Larsen, E.H. 1986. Membrane potentials and intracellular Cl activity of toad skin epithelium in relation to activation of the transepithelial Cl conductance. *J. Membrane Biol.* **94:**173–190